CHAPTER

3

Optimal and Adaptive MIMO Waveform Design

Joseph R. Guerci

Chapter Outline

3.1 INTRODUCTION

Recent advances in radar front-end hardware such as solid-state transmitters, digital arbitrary waveform generators (DAWGs), active electronically scanned arrays (AESAs), and high-performance embedded computing (HPEC) have afforded an opportunity to reexamine the design of what and how a radar transmits its spatio-temporal radio frequency (RF) signals. Conventional modern radars generally use nonadaptive transmit configurations that typically optimize some metric associated with a multidimensional ambiguity function (e.g., range, Doppler, angle [1]) and do not adapt the transmitter to an ever-changing target and interference channel. Common examples include the very popular constant modulus linear frequency modulated (LFM) waveform and low sidelobe transmit antennas [1]. However, since the output signal-to-interference-plus-noise ratio (SINR) depends on the transmit characteristics, it is natural to ask: for a given channel model, what is the optimum transmit/receive configuration?

Adaptive processing has long been implemented in the receive chain of radar, beginning with automatic gain control and cell-averaging constant false alarm rate (CA-CFAR) [2] all the way to today's space-time adaptive processing (STAP) [3]. However, adaptivity in the transmit chain is virtually nonexistent, save for mode adaptivity such as switching in different nonadaptive waveforms such as pulse repetition frequency (PRF) and bandwidth. This chapter develops the basic theory of optimal transmit/receive design using

a multi-input, multi-output (MIMO) formulation that can account for all potential degrees of freedom (DOFs) such as waveform (fast-time), angle, and polarization. Various applications and examples are provided to further illustrate the potential impact of joint transmit/receive adaptivity.

3.1.1 Organization

This chapter is organized as follows. Section 3.2 introduces the basic MIMO channel formulation and derives the optimal transmitter/receiver configuration for the additive colored noise (ACN) case. Several examples exercising different DOFs (fast-time, spatial) are then presented to illustrate the basic theory and demonstrate the flexibility of the formulation. Next in Section 3.3, the formalism is extended to account for the basic maximizing signal-to-clutter ratio (SCR) problem. In Section 3.4, a basic theory for optimizing transmit/receive configuration for the target ID problem is introduced. The concept of constrained MIMO waveform design is addressed in Section 3.5 to account for important real-world constraints such as constant modulus. Finally, in Section 3.6, the idea of adaptive MIMO waveform design is introduced when the channel must be estimated on the fly.

3.1.2 Key Points

- Fundamental theory for optimum MIMO waveform design
- MIMO waveforms for maximum SINR (additive colored noise case)
- MIMO waveforms for maximizing signal to clutter
- MIMO waveforms for target ID
- Constrained optimum MIMO waveform design
- Adaptive MIMO waveform design

3.1.3 Acronyms

Acronyms that are commonly used in this chapter include the following:

ACN	additive colored noise
AGCN	additive Gaussian colored noise
AOA	angle-of-arrival
CA-CFAR	cell-averaging constant false alarm ratio
CNR	clutter-to-noise ratio
DOFs	degrees-of-freedom
FIR	finite impulse response
GMTI	ground moving target indication
HVT	high value target
i.i.d	independent and identically distributed
LTI	Linear Time Invariant
PRF	pulse repetition frequency
Rx	receiver
SAR	synthetic aperture radar
SCR	signal-to-clutter ratio
SINR	signal-to-interference-plus-noise ratio
SNR	signal-to-noise ratio
STAP	space-time adaptive processing
Tx	transmitter
ULA	uniform linear array

3.2 | OPTIMUM MIMO WAVEFORM DESIGN FOR THE ADDITIVE COLORED NOISE CASE

Consider the basic radar block diagram in Figure 3-1. A generally complex-valued and multidimensional transmit signal, $\mathbf{s} \in \mathbb{C}^N$, (i.e., an N-dimensional multi-input (MI) signal), interacts with a target denoted by the target transfer matrix $H_T \in \mathbb{C}^{M\times N}$. The resulting M-dimensional multi-output (MO) signal (echo), $\mathbf{y} \in \mathbb{C}^M$, is then received along with ACN $\mathbf{n} \in \mathbb{C}^M$. The vector–matrix formulation is completely general inasmuch as any combination of spatial and temporal dimensions can be represented.

For example, the N-dimensional input vector $\mathbf{s}$ could represent the N complex (i.e., in-phase/quadrature, or I/Q [4]) samples of a single-channel transmit waveform $s(t)$, that is,

$$\mathbf{s} = \begin{bmatrix} s(\tau_1) \\ s(\tau_2) \\ \vdots \\ s(\tau_N) \end{bmatrix} \tag{3.1}$$

The corresponding target transfer matrix, H_T, would thus contain the corresponding samples of the complex target impulse response, $h_T(t)$, which for the causal linear time-invariant (LTI) case would have the form [5]

$$H_T = \begin{bmatrix} h[0] & 0 & 0 & \cdots & 0 \\ h[1] & h[0] & 0 & \cdots & 0 \\ h[2] & h[1] & h[0] & \cdots & 0 \\ \vdots & & & \ddots & \vdots \\ h[N-1] & & & h[1] & h[0] \end{bmatrix} \tag{3.2}$$

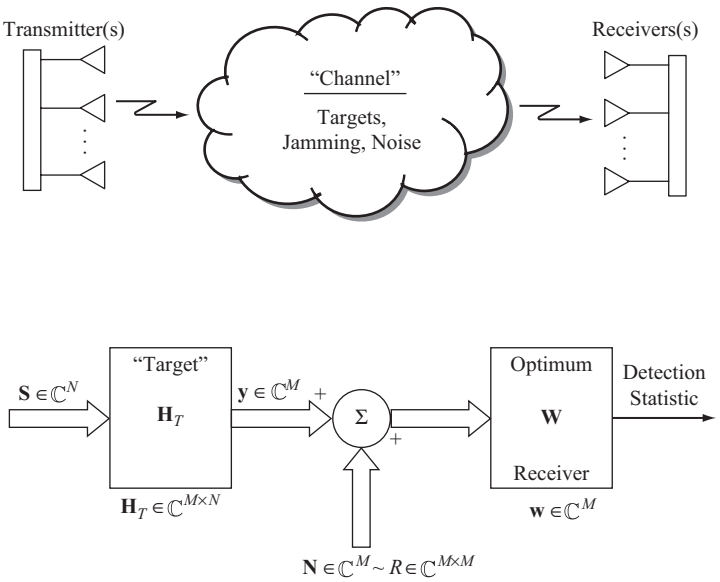

FIGURE 3-1 Fundamental multichannel radar block diagram for the AGCN case. Our objective is to design both the transmit (i.e., **s**) and receive (i.e., **w**) functions so as to maximize the output SINR given the channel characteristics.

Without loss of generality we have assumed uniform time sampling, that is, $\tau_k = (k-1)T$, where T is a suitably chosen sampling interval [6]. Note also that for convenience and a significant reduction in mathematical nomenclature overhead $N = M$ is used, which is the same number of transmit/receive DOF (e.g., time, space). The reader is encouraged to, where desired, reinstate the inequality and confirm that the underlying equations derived throughout this chapter have the same basic form except for differing vector and matrix dimensionalities. Also note that in general H_T is stochastic.

The formalism is readily extensible to the multiple-transmitter, multiple-receiver case. For example, if there are three independent transmit/receive channels (e.g., an AESA), then the input vector $\mathbf{s}$ of Figure 3-1 would have the form

$$\mathbf{s} = \begin{bmatrix} \mathbf{s}_1 \\ \mathbf{s}_2 \\ \mathbf{s}_3 \end{bmatrix} \in \mathbb{C}^{3N} \tag{3.3}$$

where $\mathbf{s}_i \in \mathbb{C}^N$ denotes the samples (as in (3.1)) of the transmitted waveform out of the i-th transmit channel. The corresponding target transfer matrix would in general have the form

$$H_T = \begin{bmatrix} H_{11} & H_{12} & H_{13} \\ H_{21} & H_{22} & H_{23} \\ H_{31} & H_{32} & H_{33} \end{bmatrix} \in \mathbb{C}^{3N \times 3N} \tag{3.4}$$

where the submatrix $H_{i,j} \in \mathbb{C}^{N \times N}$ is the transfer matrix between the i-th receive and j-th transmit channels for all time samples of the waveform.

These examples make clear that the matrix–vector, input–output formalism is completely universal and can accommodate whatever transmit/receive DOF desired. Returning to Figure 3-1, we now wish to jointly optimize the transmit/receive functions. We will find it convenient to work backward: to begin by optimizing the receiver as a function of the input and then finally optimizing the input and thus the overall output SINR.

For any finite norm input $\mathbf{s}$, the receiver that maximizes output SINR for the ACN case is the so-called whitening (or colored noise) matched filter, as shown in Figure 3-2 [7]. Note that for the additive Gaussian colored noise (AGCN) case, this receiver is also statistically optimum [7].

If $R \in \mathbb{C}^{N \times N}$ denotes the total interference covariance matrix associated with $\mathbf{n}$, which is further assumed to be independent of $\mathbf{s}$ and Hermitian positive definite [8] (guaranteed in practice due to ever-present receiver noise [7]), then the corresponding whitening filter

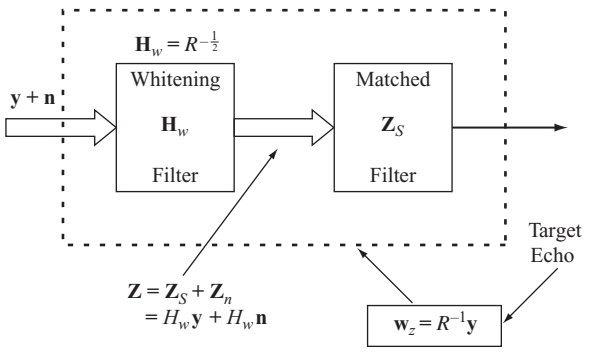

FIGURE 3-2 ■ The optimum receiver for the ACN case consists of a whitening filter followed by a white noise matched filter.

is given by [7]:

$$H_w = R^{-\frac{1}{2}} \tag{3.5}$$

The reader should verify the whitening properties of (3.5) (see problem 2 and [9]).

The output of the linear whitening filter, $\mathbf{z} \in \mathbb{C}^N$, will consist of signal and noise components, $\mathbf{z}_s$, $\mathbf{z}_n$, respectively, given by

$$\begin{aligned} \mathbf{z} &= \mathbf{z}_s + \mathbf{z}_n \\ &= H_w \mathbf{y}_s + H_w \mathbf{n} \\ &= H_w H_T \mathbf{s} + H_w \mathbf{n} \end{aligned} \tag{3.6}$$

where $\mathbf{y}_s \in \mathbb{C}^N$ denotes the target echo as shown in Figure 3-2 (i.e., the output of H_T).

Since the noise has been whitened via a linear—in this case full-rank—transformation [7]), the final receiver stage consists of a white noise matched filter of the form (to within a multiplicative scalar)

$$\mathbf{w}_z = \mathbf{z}_s \in \mathbb{C}^N \tag{3.7}$$

The corresponding output SNR is thus given by

$$\begin{aligned} \mathrm{SNR}_o &= \frac{\left|\mathbf{w}'_z \mathbf{z}_s\right|^2}{\mathrm{var}\left(\mathbf{w}'_z \mathbf{z}_n\right)} \\ &= \frac{\left|\mathbf{z}'_s \mathbf{z}_s\right|^2}{\mathrm{var}\left(\mathbf{z}'_s \mathbf{z}_n\right)} \\ &= \frac{\left|\mathbf{z}'_s \mathbf{z}_s\right|^2}{E\{\mathbf{z}'_s \mathbf{z}_n \mathbf{z}'_n \mathbf{z}_s\}} \\ &= \frac{\left|\mathbf{z}'_s \mathbf{z}_s\right|^2}{\mathbf{z}'_s E\{\mathbf{z}_n \mathbf{z}'_n\} \mathbf{z}_s} \\ &= \frac{\left|\mathbf{z}'_s \mathbf{z}_s\right|^2}{\mathbf{z}'_s \mathbf{z}_s} \\ &= \left|\mathbf{z}'_s \mathbf{z}_s\right| \end{aligned} \tag{3.8}$$

where $\mathrm{var}(\cdot)$ denotes the variance. Note that due to the whitening operation $E\left\{\mathbf{z}_n \mathbf{z}'_n\right\} = I$.

In words, the output SNR is proportional to the energy in the whitened target echo. This fact is key to optimizing the input function: Chose $\mathbf{s}$ (the input) to maximize the energy in the whitened target echo:

$$\max_{\{\mathbf{s}\}} \quad \left|\mathbf{z}'_s \mathbf{z}_s\right| \tag{3.9}$$

Substituting $\mathbf{z}_s = H_w H_T \mathbf{s}$ into (3.9) yields the objective function that explicitly depends on the input

$$\max_{\{\mathbf{s}\}} \quad \left|\mathbf{s}' \left(H' H\right) \mathbf{s}\right| \tag{3.10}$$

where

$$H \triangleq H_w H_T \tag{3.11}$$

Recognizing that (3.10) involves the magnitude of the inner product of two vectors $\mathbf{s}$ and $(H'H)\mathbf{s}$, we readily have from the Cauchy–Schwarz theorem [10] the condition that $\mathbf{s}$ must satisfy to yield a maximum, namely, $\mathbf{s}$ *must be collinear with* $(H'H)\mathbf{s}$:

$$\left(H'H\right)\mathbf{s}_{opt} = \lambda_{max}\mathbf{s}_{opt} \tag{3.12}$$

In other words, the optimum input $\mathbf{s}_{opt}$ must be an eigenvector of $(H'H)$ with associated maximum eigenvalue.

The previous set of input–output design equations represents the absolute optimum that any combination of transmit/receive operations can achieve and thus are fundamentally important in ascertaining the value of advanced adaptive methods (e.g., adaptive waveforms, transmit/receive beamforming). Note also that (3.12) can be generalized to the case where the target response is random:

$$E\left\{H'H\right\}\mathbf{s}_{opt} = \lambda_{max}\mathbf{s}_{opt} \tag{3.13}$$

In this case, $\mathbf{s}_{opt}$ maximizes the expected value of the output SINR.

Next we illustrate the application of the previously given optimum design equations to the additive colored noise problem arising from a broadband multipath interference source.

EXAMPLE 3.1

Additive Colored Noise Example Arising from Broadband Multipath Interference

This example illustrates the optimum transmit/receive configuration for maximizing output SINR in the presence of colored noise interference arising from a multipath broadband noise source. More specifically, for the single transmit/receive channel case, it derives the optimum transmit pulse modulation (i.e., pulse shape).

Figure 3-3 illustrates a nominally broadband white noise source undergoing a series of multipath scatterings that in turn colors the noise spectrum [11]. Assuming (for simplicity) that the multipath reflections are dominated by several discrete specular reflections, the resultant signal can be viewed as the output of a causal tapped delay line filter (i.e., an FIR filter [5]) of the form

$$h_{mp}[k] = \alpha_0\delta[k] + \alpha_1\delta[k-1] + \cdots + \alpha_{q-1}\delta[k-q-1] \tag{3.14}$$

that is driven by white noise. The corresponding input–output transfer $H_{mp} \in \mathbb{C}^{N\times N}$ is thus given by

$$H_{mp} = \begin{bmatrix} h_{mp}[0] & 0 & \cdots & 0 \\ h_{mp}[1] & h_{mp}[0] & & \vdots \\ \vdots & & \ddots & 0 \\ h_{mp}[N-1] & \cdots & h_{mp}[1] & h_{mp}[0] \end{bmatrix} \tag{3.15}$$

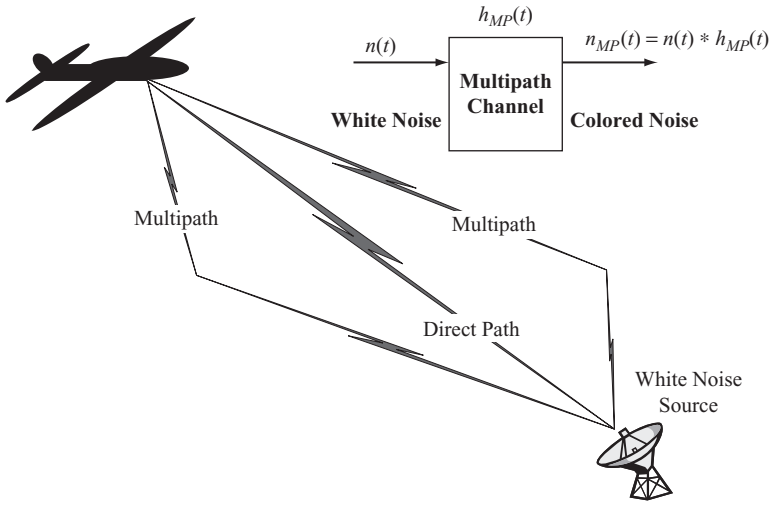

FIGURE 3-3 ■ Illustration of colored noise interference resulting from a broadband (i.e., white noise) source undergoing multipath reflections.

In terms of the multipath transfer matrix, H_{mp}, the colored noise interference covariance matrix is given by

$$\begin{aligned} E\{\mathbf{n}\mathbf{n}'\} &= E\{H_{mp}\mathbf{v}\mathbf{v}'H'_{mp}\} \\ &= H_{mp}E\{\mathbf{v}\mathbf{v}'\}H'_{mp} \\ &= H_{mp}H'_{mp} \\ &= R \end{aligned} \tag{3.16}$$

where the driving white noise source $\mathbf{v} \in \mathbb{C}^N$ is a zero mean complex vector random variable with an identity covariance matrix:

$$E\{\mathbf{v}\mathbf{v}'\} = I \tag{3.17}$$

Assuming a unity gain point target at the origin, that is, $h_T[k] = \delta[k]$, yields a target transfer matrix $H_T \in C^{N\times N}$ given by

$$\begin{aligned} H_T &= \begin{bmatrix} h_T[0] & 0 & \cdots & 0 \\ h_T[1] & h_T[0] & & \vdots \\ \vdots & & \ddots & 0 \\ h_T[N-1] & \cdots & h_T[1] & h_T[0] \end{bmatrix} \\ &= I \end{aligned} \tag{3.18}$$

While certainly a more complex (and thus realistic) target model could be assumed, we wish to focus on the impact the colored noise has on shaping the optimum transmit pulse. We will introduce more complex target response models in the target ID section.

Figure 3-4 shows the in-band interference spectrum for the case when $\alpha_0 = 1, \alpha_2 = 0.9, \alpha_5 = 0.5, \alpha_{10} = 0.2$, and all other coefficients are set to zero. The total number of fast-time (range bin) samples was set to both a short-pulse case of $N = 11$ (Figure 3-4a) and a long-pulse case of $N = 100$ (Figure 3-4b). Note that the multipath colors the otherwise flat noise spectrum. Also displayed is the spectrum of a conventional (and thus nonoptimized) LFM pulse with a time–bandwidth product, $\beta\tau$, of 5 (Figure 3-4a) and 50 (Figure 3-4b), respectively [12, 13].

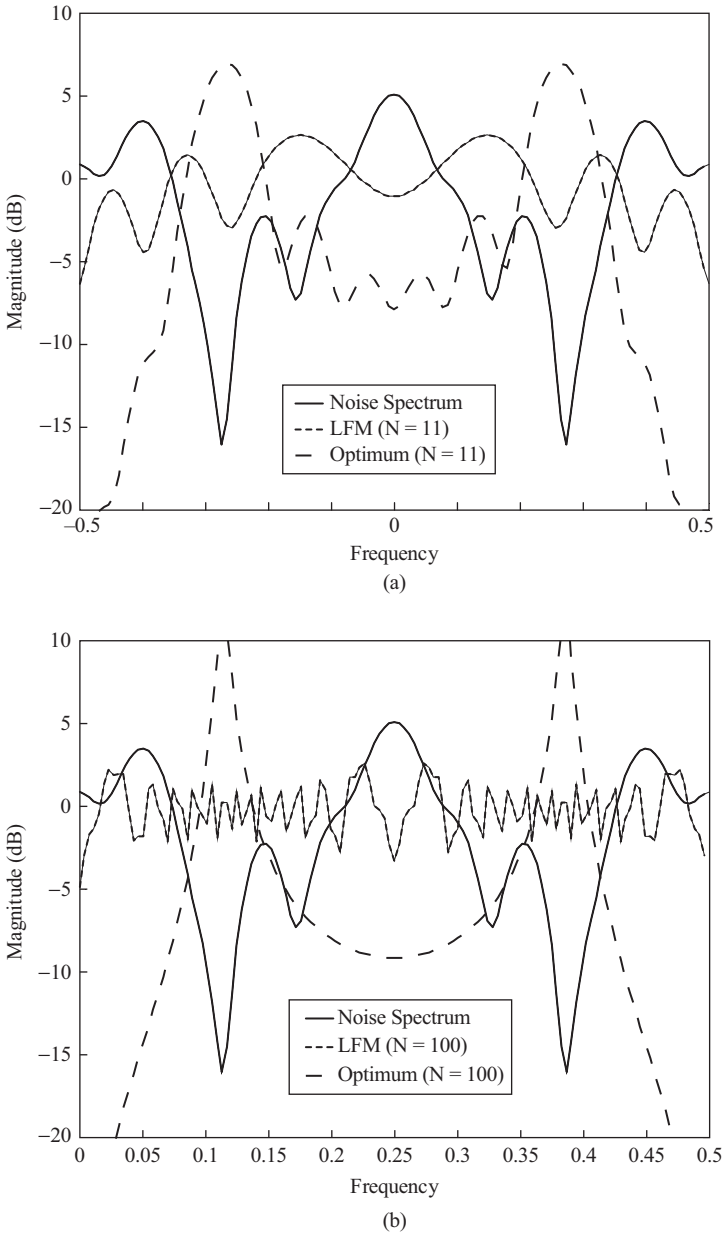

FIGURE 3-4 ■ Spectra of the colored noise interference along with conventional and optimal pulse modulations. (a) Short-pulse case where total duration for the LFM and optimum pulse are set to 11 range bins (fast-time taps). (b) Long-pulse case where total duration for the LFM and optimum pulse are set to 100 range bins. Note that in both cases the optimum pulse attempts to anti-match to the colored noise spectrum under the frequency resolution constraint set by the total pulse width.

Given R from (3.16), the corresponding whitening filter $H_w$is given by

$$H_w = R^{-\frac{1}{2}} \tag{3.19}$$

Combining (3.19) with (3.18), the total composite channel transfer matrix H is thus given by

$$H = H_w H_T = H_w = R^{-\frac{1}{2}} \tag{3.20}$$

Substituting (3.20) into (3.12) yields

$$R^{-1}\mathbf{s}_{opt} = \lambda \mathbf{s}_{opt} \tag{3.21}$$

That is, the optimum transmit waveform is the maximum eigenfunction associated with the inverse of the interference covariance matrix. The reader should verify that this is also the minimum eigenfunction of the original covariance matrix R and thus can be computed without matrix inversion.

Displayed in Figures 3-4a and 3-4b are the spectra of the optimum transmit pulses obtained by solving (3.21) for the maximum eigenfunction–eigenvalue pair for the aforementioned short- and long-pulse cases, respectively. Note how the optimum transmit spectrum naturally emphasizes portions of the spectrum where the interference is weak—which is an intuitively satisfying result.

The SINR gain of the optimum short pulse, SINR_{opt}, relative to that of a nonoptimized chirp pulse, SINR_{LFM}, is

$$\text{SINR}_{gain} \triangleq \frac{\text{SINR}_{opt}}{\text{SINR}_{LFM}} = 7.0 \text{ dB} \tag{3.22}$$

while for the long-pulse case

$$\text{SINR}_{gain} \triangleq \frac{\text{SINR}_{opt}}{\text{SINR}_{LFM}} = 24.1 \text{ dB} \tag{3.23}$$

The increase in SINR for the long-pulse case is to be expected since it has finer spectral resolution and can therefore more precisely shape the transmit modulation to antimatch the interference. Of course, the unconstrained optimum pulse has certain practical deficiencies (e.g., poorer resolution, compression sidelobes) compared with a conventional pulse. We will revisit these issues in Section 3.5 where constrained optimization is introduced.

Example 3.1 is similar in spirit to the spectral notching waveform design problem that arises when strong co-channel narrowband interferers are present [14]. In this case it is desirable not only to filter out the interference on receive but also to choose a transmit waveform that minimizes energy in the co-channel bands. The reader is encouraged to experiment with different notched spectra and pulse length assumptions and to apply (3.12) as in example 3.1. Non-impulsive target models can also be readily incorporated.

3.3 | OPTIMUM MIMO DESIGN FOR MAXIMIZING SIGNAL-TO-CLUTTER RATIO

The joint MIMO optimization of the transmit and receive functions for the general additive colored noise plus clutter (signal-dependent noise) has been shown to result in a highly nonlinear problem [15] (though efficient iterative methods have been developed to solve these equations [15]). In practice, however, there is often a natural "separation principle" between additive colored noise (signal independent) and clutter (signal dependent). For example, narrowband electromagnetic interference (EMI) resulting from co-channel interference might require fast-time receiver and transmit spectral notching [14], leaving the slow-time or spatial DOF available for clutter suppression. Similarly, adaptive beamforming for broadband jammer nulling can be separated from the clutter suppression problem in a two-stage approach (see, e.g., [16]). We will thus concentrate in this section on the clutter dominant case and focus solely on maximizing the output signal-to-clutter ratio (SCR).

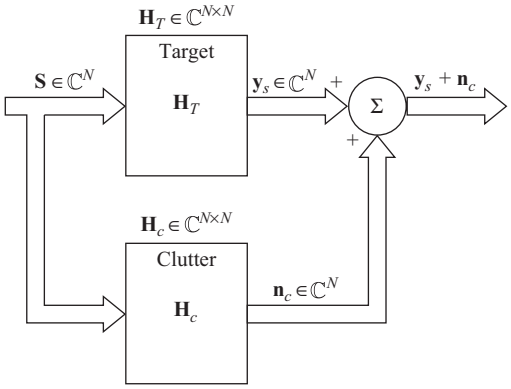

FIGURE 3-5 ■ Radar signal block diagram for the clutter dominant case illustrating the direct dependency of the clutter signal on the transmitted signal.

Unlike the previous colored noise case in Section 3.2, clutter (i.e., channel reverberations) is a form of signal-dependent noise [17, 18] since the clutter returns depend on the transmit signal characteristics (e.g., transmit antenna pattern and strength, operating frequencies, bandwidths, polarization). Referring to Figure 3-5, the corresponding SCR at the input to the receiver is given by

$$\begin{aligned} \text{SCR} &= \frac{E\{\mathbf{y}'_T \mathbf{y}_T\}}{E\{\mathbf{y}'_c \mathbf{y}_c\}} \\ &= \frac{\mathbf{s}' E\{H'_T H_T\}\mathbf{s}}{\mathbf{s}' E\{H'_c H_c\}\mathbf{s}} \end{aligned} \tag{3.24}$$

where $H_c \in \mathbb{C}^{N\times N}$ denotes the clutter transfer matrix, which is generally taken to be stochastic. Equation (3.24) is a generalized Rayleigh quotient [8] that is maximized when $\mathbf{s}$ is a solution to the generalized eigenvalue problem

$$E\{H'_T H_T\}\mathbf{s} = \lambda E\{H'_c H_c\}\mathbf{s} \tag{3.25}$$

with corresponding maximum eigenvalue. When $E\{H'_c H_c\}$ is positive definite, (3.25) can be converted to an ordinary eigenvalue problem of the form we have already encountered, specifically,

$$E\{H'_c H_c\}^{-1} E\{H'_T H_T\}\mathbf{s} = \lambda \mathbf{s} \tag{3.26}$$

Applying equations (3.25) and (3.26) to the full-up space-time clutter suppression of ground moving target indicator (GMTI) clutter is available in [19]. Due to space limitations, we will instead consider its application to the sidelobe target suppression problem, which is very closely related to the ground clutter interference issue.

EXAMPLE 3.2

Sidelobe Target Suppression

Consider a narrowband $N = 16$ element uniform linear array (ULA) with half-wavelength interelement spacing and a quiescent pattern (Figure 3-6). In addition to the desired target at

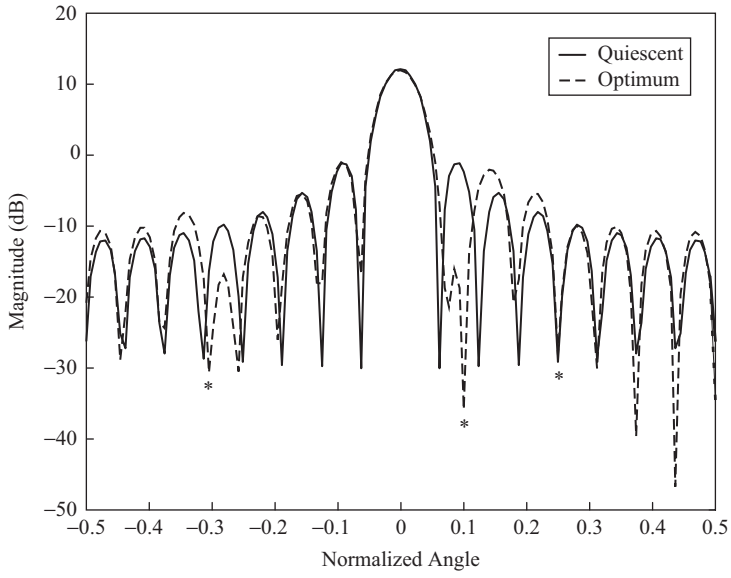

FIGURE 3-6 ■ Illustration of proactive sidelobe target blanking on transmit achieved by maximizing the SCR. Note the presence of nulls in the directions of competing targets while preserving the desired mainbeam response.

a normalized angle of $\bar{\theta} = 0$, there are strong sidelobe targets at $\bar{\theta}_1 = -0.3, \bar{\theta}_2 = +0.1, \bar{\theta}_3 = +0.25$, where a normalized angle is defined as

$$\bar{\theta} \triangleq \frac{d}{\lambda} \sin\theta \tag{3.27}$$

In (3.27) d is the interelement spacing of the ULA, and λ is the operating wavelength (consistent units and narrowband operation assumed).

The presence of these targets (possibly large clutter discretes) could have been previously detected, thus making their AOAs are known. Also, their strong sidelobes could potentially mask weaker mainlobe targets. With this knowledge, it is desired to minimize any energy from these targets leaking into the mainbeam detection of the target of interest by nulling on transmit, or placing transmit antenna pattern nulls in the directions of the unwanted targets.

For the case at hand, the (m, n)-th elements of the target and interferer transfer matrices are given, respectively, by

$$[H_T]_{m,n} = e^{j\varphi} \text{ (const.)} \tag{3.28}$$

$$[H_c]_{m,n} = \alpha_1 e^{j2\pi(m-n)\bar{\theta}_1} + \alpha_2 e^{j2\pi(m-n)\bar{\theta}_2} + \alpha_3 e^{j2\pi(m-n)\bar{\theta}_3} \tag{3.29}$$

where φ is an overall bulk delay (two way propagation) that does not affect the solution to (3.25) and will thus be subsequently ignored, and $[H_c]_{m,n}$ is the (m, n)-th element of the clutter transfer matrix and consists of the linear superposition of the three target returns resulting from transmitting a narrowband signal from the n-th transmit element and receiving it on the m-th receive element of a ULA that uses the same array for transmit and receive [3, 13]. Note that in practice there would be a random relative phase between the signals in (3.29), which for convenience we have ignored but which can easily be accommodated by taking the expected value of the kernel $H_c' H_c$.

Solving (3.25) for the optimum eigenvector yields the transmit pattern that maximizes the SCR, which is the pattern also displayed in Figure 3-6. The competing target amplitudes were set to 40 dB relative to the desired target and 0 dB of diagonal loading was added to $H_c' H_c$ to improve numerical conditioning and allow for its inversion. Although this is somewhat

arbitrary, it does provide a mechanism for controlling null depth, that in practice is limited by the amount of transmit channel mismatch [20]. Note the presence of transmit antenna pattern nulls in the directions of the competing targets as desired.

EXAMPLE 3.3

Optimal Pulse Shape for Maximizing SCR

In this simple example, we rigorously verify an intuitively obvious result regarding pulse shape and detecting a point target in uniform clutter: the best waveform for detecting a point target in independent and identically distributed (i.i.d) clutter is itself an impulse (i.e., a waveform with maximal resolution), a well-known result rigorously proven by Manasse [21] using a different method.

Consider a unity point target, arbitrarily chosen to be at the temporal origin. Its corresponding impulse response and transfer matrix are respectively given by

$$h_T[n] = \delta[n] \tag{3.30}$$

and

$$H_T = I_{N\times N} \tag{3.31}$$

where $I_{N\times N}$ denotes the $N \times N$ identity matrix. For uniformly distributed clutter, the corresponding impulse response is of the form

$$h_c[n] = \sum_{k=0}^{N-1} \tilde{\gamma}_k \delta[n-k] \tag{3.32}$$

where $\tilde{\gamma}_i$ denotes the complex reflectivity random variable of the clutter contained in the i-th range cell (i.e., fast-time tap). The corresponding transfer matrix is given by

$$\tilde{H}_c = \begin{bmatrix} \tilde{\gamma}_0 & 0 & 0 & \cdots & 0 \\ \tilde{\gamma}_1 & \tilde{\gamma}_0 & & & \\ \tilde{\gamma}_2 & \tilde{\gamma}_1 & \tilde{\gamma}_0 & & \\ \vdots & & & \ddots & \\ \tilde{\gamma}_{N-1} & \tilde{\gamma}_{N-2} & \tilde{\gamma}_{N-3} & \cdots & \tilde{\gamma}_0 \end{bmatrix} \tag{3.33}$$

Assuming that the $\tilde{\gamma}_i$ values are i.i.d., we have

$$E\left\{\tilde{\gamma}_i^* \tilde{\gamma}_j\right\} = P_c \delta[i-j] \tag{3.34}$$

and thus

$$E\left\{\left[\tilde{H}_c' \tilde{H}_c\right]_{i,j}\right\} = \begin{cases} 0, & i \neq j \\ (N+1-i)P_c, & i = j \end{cases} \tag{3.35}$$

where $[]_{i,j}$ denotes the (i, j)-th element of the transfer matrix. Note that (3.35) is also diagonal (and thus invertible), but with nonequal diagonal elements.

Finally, substituting (3.31) and (3.35) into (3.26) yields

$$E\left\{\tilde{H}_c' \tilde{H}_c\right\}^{-1} \mathbf{s} = \lambda \mathbf{s} \tag{3.36}$$

where

$$E\left\{\tilde{H}_c'\tilde{H}_c\right\}^{-1} = \frac{1}{P_c}\begin{bmatrix} d_1 & 0 & \cdots & 0 \\ 0 & d_2 & & \\ & & \ddots & \\ 0 & & \cdots & d_N \end{bmatrix} \tag{3.37}$$

and

$$d_i \triangleq (N+i-1)^{-1} \tag{3.38}$$

It is readily verified that the solution to (3.36) yielding the maximum eigenvalue is given by

$$\mathbf{s} = \begin{bmatrix} 1 \\ 0 \\ \vdots \\ 0 \end{bmatrix} \tag{3.39}$$

Thus the optimum pulse shape for detecting a point target is itself an impulse. This should be immediately obvious since it is the shape that excites the range bin only with the target and zeros out all other range bin returns that contain competing clutter.

Of course, transmitting a short pulse (much less an impulse) is problematic in the real world (e.g., creating extremely high peak power pulses) thus an approximation to a short pulse in the form of a spread spectrum waveform (e.g., LFM) is often employed [12]. This example also illuminates that in uniform random clutter nothing is gained by sophisticated pulse shaping for a point target other than to maximize bandwidth (i.e., range resolution) [21]. The interested reader is referred to [19] for further examples of optimizing other DOF (e.g., angle-Doppler) for the clutter mitigation problem.

Up to this point we have been focused on judiciously choosing the transmit/receive DOF to maximize SINR or SCR. In the next section we will extend this framework to the target identification problem.

3.4 | OPTIMUM MIMO DESIGN FOR TARGET IDENTIFICATION

Consider the problem of determining target type when two possibilities exist (the multitarget case is addressed later in this section). This can be cast as a classical binary hypothesis testing problem [7]:

$$\begin{array}{lll} \text{(Target 1)} & \mathrm{H}_1: & \mathbf{y}_1 + \mathbf{n} = H_{T_1}\mathbf{s} + \mathbf{n} \\ \text{(Target 2)} & \mathrm{H}_2: & \mathbf{y}_2 + \mathbf{n} = H_{T_2}\mathbf{s} + \mathbf{n} \end{array} \tag{3.40}$$

where H_{T_1}, H_{T_2} denote the target transfer matrices for targets 1 and 2, respectively. For the AGCN case, the well-known optimum receiver decision structure consists of a bank of matched filters, each tuned to a different target assumption, followed by comparator as shown in Figure 3-7 [7]. Note that (3.40) presupposes that either Target 1 or 2 is present, but

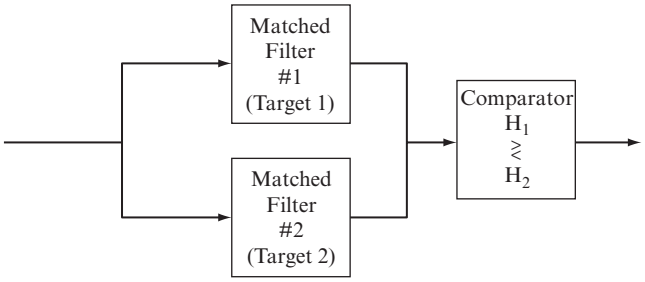

FIGURE 3-7 ■ Optimal receiver structure for the binary (two-target) hypothesis testing AGCN problem.

not both. Also, it has been tacitly assumed that a binary detection test has been conducted to ensure that a target is indeed present [7]. Alternatively, the null hypothesis (no target present) can be included in the test as a separate hypothesis.

Figure 3-8 illustrates the situation at hand. If Target-1 is present, the observed signal $\mathbf{y}_1+\mathbf{n}$ will tend to cluster about the #1 point in observation space—which could include any number of dimensions relevant to the target ID problem (e.g., fast-time, angle, Doppler, polarization). The uncertainty sphere (generally ellipsoid for AGCN case) surrounding #1 in Figure 3-7 represents the 1-sigma probability for the additive noise $\mathbf{n}$—and similarly for #2. Clearly, if $\mathbf{y}_1$ and $\mathbf{y}_2$ are relatively well separated, the probability of correct classification is commensurately high.

Significantly, $\mathbf{y}_1$ and $\mathbf{y}_2$ depend on the transmit signal $\mathbf{s}$, as shown in (3.40). Consequently, it should be possible to select an $\mathbf{s}$ that maximizes the separation between $\mathbf{y}_1$ and $\mathbf{y}_2$, thereby maximizing the probability of correct classification under modest assumptions regarding the conditional probability density functions (PDFs) (e.g., unimodality), that is,

$$\max_{\{\mathbf{s}\}} \quad \left|\mathbf{d}'\mathbf{d}\right| \tag{3.41}$$

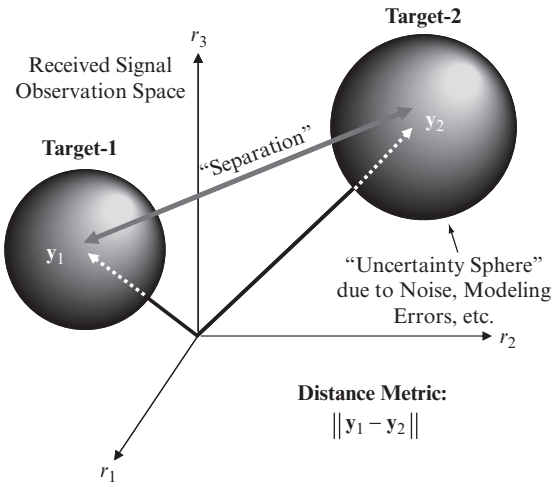

FIGURE 3-8 ■ Illustration of the two-target ID problem. The goal of the joint transmitter/receiver design is to maximally separate the received signals in observation space, which in turn maximizes the probability of correct classification for the additive unimodal monotonic distributed noise case (e.g., AGCN).

where

$$\begin{aligned}\mathbf{d} &\triangleq \mathbf{y}_1 - \mathbf{y}_2 \\ &= H_{T_1}\mathbf{s} - H_{T_2}\mathbf{s} \\ &= \left(H_{T_1} - H_{T_2}\right)\mathbf{s} \\ &\triangleq H\mathbf{s}\end{aligned} \tag{3.42}$$

and where

$$H \triangleq H_{T_1} - H_{T_2} \tag{3.43}$$

Substituting (3.42) into (3.41) yields

$$\max_{\{\mathbf{s}\}} \quad \left|\mathbf{s}'H'H\mathbf{s}\right| \tag{3.44}$$

This is precisely of the form (3.10) and thus has a solution yielding maximum separation given by

$$\left(H'H\right)\mathbf{s}_{opt} = \lambda_{max}\mathbf{s}_{opt} \tag{3.45}$$

It is noted that (3.45) has an interesting interpretation: $\mathbf{s}_{opt}$ is that transmit input that maximally separates the target responses and is thus the maximum eigenfunction of the transfer kernel $H'H$ formed by the difference between the target transfer matrices (i.e., (3.43)). Again if the composite target transfer matrix is stochastic, $H'H$ is replaced with its expected value $E\left\{H'H\right\}$ in (3.45).

EXAMPLE 3.4

Two-Target Identification Example

Let $h_1[n]$ and $h_2[n]$ denote the impulse responses of targets #1 and #2, respectively (Figure 3-9). Figure 3-10 shows two different (normalized) transmit waveforms—LFM and optimum (per (3.46))—along with their corresponding normalized separation norms of 0.45 and 1,

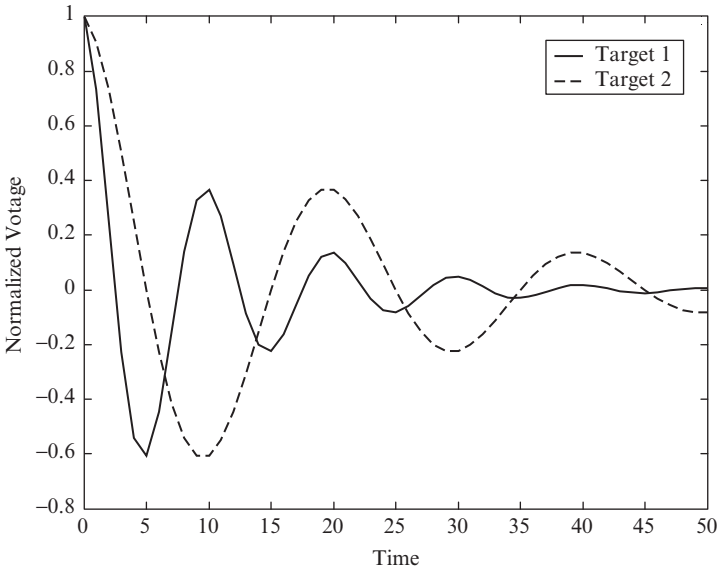

FIGURE 3-9 ■ Target impulse responses utilized for the two-target identification problem.

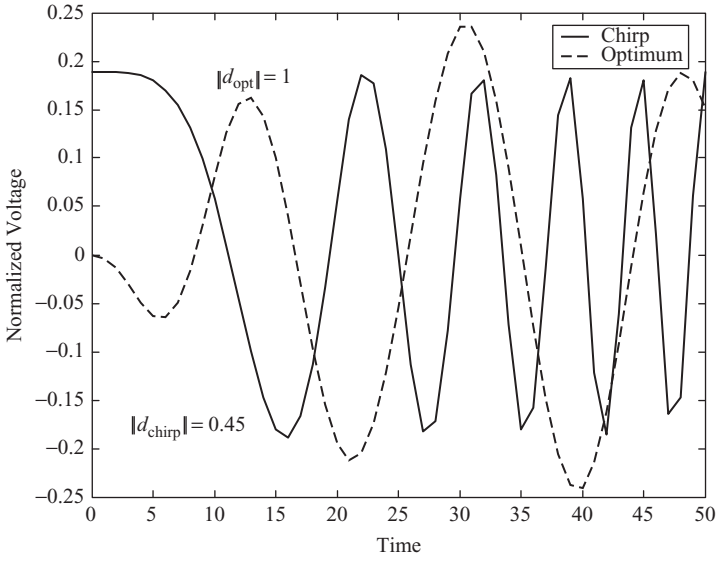

FIGURE 3-10 ■ Transmit waveforms employed in the two-target identification example.

respectively, which corresponds to 6.9 dB improvement in separation. To determine the relative probabilities of correct classification for the different transmit waveforms, one would first need to set the SNR level, which fixes the conditional PDF herein assumed to be circular Gaussian, and then to measure the amount of overlap to calculate the probability [7].

An examination of Figure 3-11 reveals the mechanism by which enhanced separation is achieved. It shows the Fourier spectrum of $H(\omega) = H_{T_1}(\omega) - H_{T_2}(\omega)$, along with that of $S_{opt}(\omega)$. Note that $S_{opt}(\omega)$ places more energy in spectral regions where $H(\omega)$ is large (i.e., spectral regions where the difference between targets is large, which is again an intuitively appealing result).

While pulse modulation was used to illustrate the optimum transmit design equations, we could theoretically have used any transmit DOF (e.g., polarization). The choice clearly depends on the application at hand.

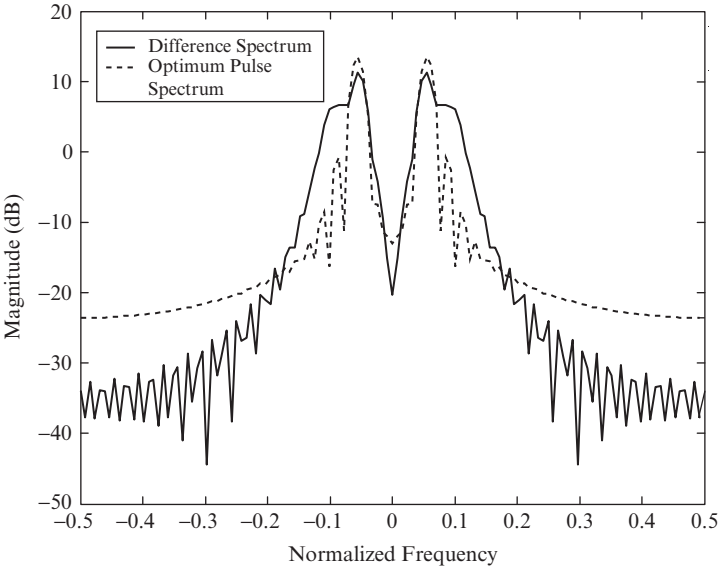

FIGURE 3-11 ■ Comparison of the two-target difference spectrum and the optimum pulse spectrum. Note that the optimum pulse emphasizes parts of the spectrum where the two targets differ the most.

Multitarget Case Given L targets in general, we wish to ensure that the L-target response spheres are maximally separated (an inverse sphere packing problem [22]). To accomplish this, we would like to jointly maximize the norms of the set of separations $\{\|\mathbf{d}_{ij}\| \mid i = 1:L;\ j = i+1:L\}$:

$$\max_{\mathbf{s}} \quad \sum_{i=1}^{L} \sum_{j=i+1}^{L} \left|\mathbf{d}'_{ij}\mathbf{d}_{ij}\right| \tag{3.46}$$

Since, by definition, $\mathbf{d}_{ij}$ is given by

$$\mathbf{d}_{ij} \triangleq \left(H_{T_i} - H_{T_j}\right)\mathbf{s} \triangleq H_{ij}\mathbf{s} \tag{3.47}$$

(3.46) can be rewritten as

$$\max_{\mathbf{s}} \quad \mathbf{s}'\left(\sum_{i=1}^{L} \sum_{j=i+1}^{L} H'_{ij}H_{ij}\right)\mathbf{s} \triangleq \mathbf{s}'K\mathbf{s} \tag{3.48}$$

Since $K \in C^{N\times N}$ is the sum of positive semidefinite matrices, it shares this same property, and thus the optimum transmit input satisfies

$$K\mathbf{s}_{opt} = \lambda_{max}\mathbf{s}_{opt} \tag{3.49}$$

EXAMPLE 3.5

Multitarget Identification

Figure 3-12 depicts the impulse responses of three different targets, two of which are the same as in Example 3.4. Solving (3.48) and (3.49) yields an optimally separating waveform

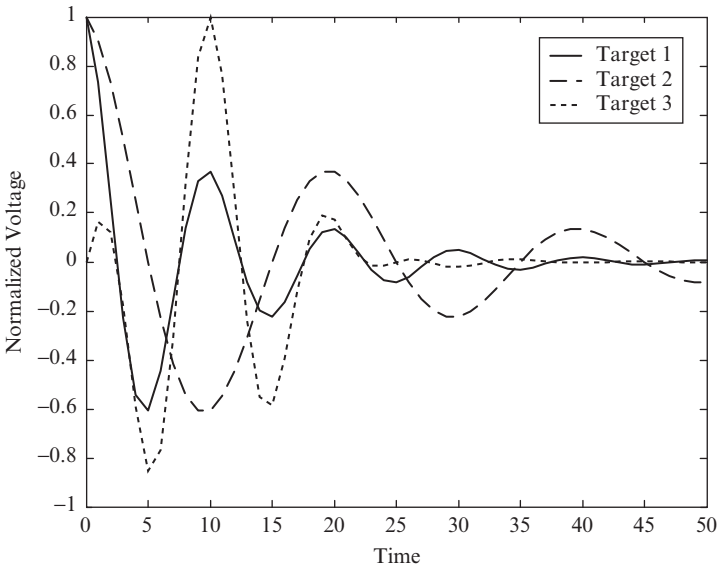

FIGURE 3-12 Target impulse responses used for the three-target identification problem.

whose average separation defined by (3.46) is 1.0. This is compared with 0.47 for the LFM of Example 3.4, an improvement of 6.5 dB, which is slightly less than the previous two-target example. As expected, the optimum waveform significantly outperforms the unoptimized pulse waveform such as the LFM.

3.5 CONSTRAINED OPTIMUM MIMO RADAR

Often there are a number of practical considerations may preclude transmitting the unconstrained optimum solutions developed so far. We will thus consider two cases of constrained optimization: linear and nonlinear.

Case 3.1: Linear Constraints

Consider the linearly constrained version of the input optimization problem:

$$\max_{\{\mathbf{s}\}} \quad \left|\mathbf{s}' H' H \mathbf{s}\right| \tag{3.50}$$

$$\text{subject to:} \quad G\mathbf{s} = \mathbf{0} \tag{3.51}$$

where $G \in \mathbb{C}^{Q\times N}$. To avoid the overly constrained case, it is assumed that $Q < N$. For example, the rows of G could represent steering vectors associated with known interferers such as unwanted targets or clutter discretes to which we wish to apply transmit nulls.

Equation (3.51) defines the feasible solution subspace for the constrained optimization problem. It is straightforward to verify that the projection operator

$$P = I - G'\left(GG'\right)^{-1} G \tag{3.52}$$

projects any $\mathbf{x} \in \mathbb{C}^N$ into the feasible subspace [23]. Thus, we can first apply the projection operator then perform an unconstrained subspace optimization to obtain the solution to (3.50) and (3.51), that is,

$$\max_{\{\mathbf{s}\}} \quad \left|\mathbf{s}' P' H' H P \mathbf{s}\right| \tag{3.53}$$

From (3.53) it is readily apparent that the constrained optimum transmit input satisfies

$$P' H' H P \mathbf{s}_{opt} = \lambda_{max} \mathbf{s}_{opt} \tag{3.54}$$

EXAMPLE 3.6

Prenulling on Transmit

If there are known AOAs for which it is desired not to transmit (e.g., unwanted targets, clutter discrete, keep-out zones), it is possible to formulate a linearly constrained optimization accordingly.

Assume that there is a desired target at $\bar{\theta}_T$ as well as two keep-out angles (normalized) $\bar{\theta}_{I_1}$ and $\bar{\theta}_{I_2}$. The corresponding elements of the target transfer matrix $H_T \in \mathbb{C}^{N\times N}$, assuming an N-element ULA, are thus given by

$$[H_T]_{m,n} = e^{j2\pi(m-n)\bar{\theta}_T} \tag{3.55}$$

where $[H_T]_{m,n}$ denotes the (m, n)-th element of the target transfer matrix.

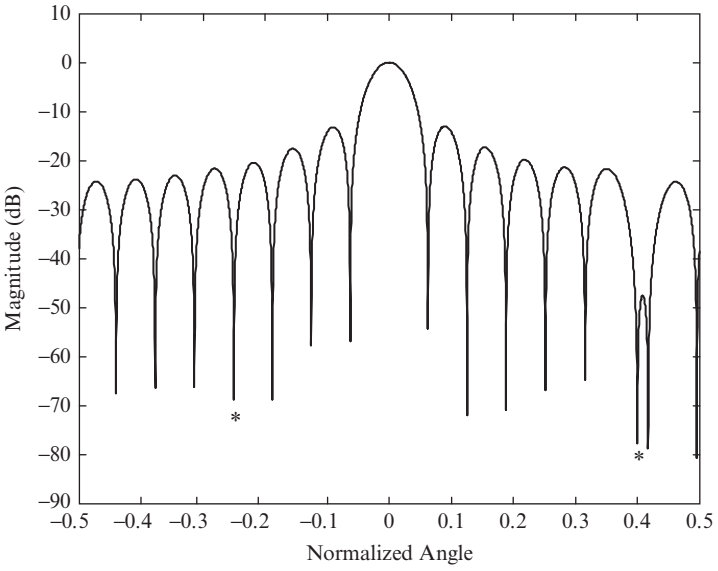

FIGURE 3-13 ■ Example of a linearly constrained optimization in which two interferers are removed via the projection optimization approach.

The keep-out constraints have the form

$$\begin{aligned}\mathbf{0} &= G\mathbf{s} \\ &= \begin{bmatrix} \mathbf{s}'_{I_1} \\ \mathbf{s}'_{I_2} \end{bmatrix} \mathbf{s}\end{aligned} \tag{3.56}$$

where

$$\mathbf{s}_{I_k} = \begin{bmatrix} 1 \\ e^{j2\pi\bar{\theta}_{I_k}} \\ \vdots \\ e^{j2\pi(N-1)\bar{\theta}_{I_k}} \end{bmatrix} \tag{3.57}$$

Figure 3-13 shows the resulting constrained optimum transmit pattern for the case where $\bar{\theta}_T = 0,\ \bar{\theta}_{I_1} = -0.25,\ \bar{\theta}_{I_2} = 0.4$. As expected a peak is placed in the desired target direction with nulls simultaneously placed in the keep-out directions.

Case 3.2: Nonlinear Constraints

In practice other generally nonlinear constraints may arise. One family of such constraints relates to the admissibility of transmit waveforms, such as the class of constant modulus and stepped frequency waveforms [12], to name but a few.

For example, if it is desired to transmit a waveform that is nominally of the LFM type (or any other prescribed type) but that is allowed to modestly deviate to better match the channel characteristics, then the nonlinear constrained optimization has the form

$$\max_{\{\mathbf{s}\}} \quad \left|\mathbf{s}' H' H \mathbf{s}\right| \tag{3.58}$$

$$\text{subject to:} \|\mathbf{s} - \mathbf{s}_{LFM}\| \leq \delta \tag{3.59}$$

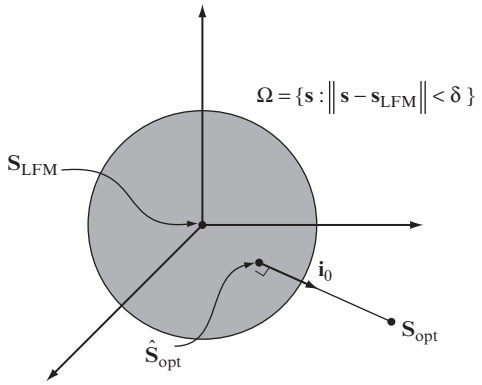

FIGURE 3-14 ■ Illustration of a constrained optimization in which the signal should lie within a subspace (in this case convex) defined to be close to a prescribed transmit input (in this case an LFM waveform). The optimum relaxed projection is the point closest to the unconstrained optimum but still residing in the subspace.

The previous and similar problems cannot generally be solved in closed form. However, approximate methods can yield satisfactory results, and we will consider two here that are based on very different approaches. These simpler methods could form the basis of more complex methods, such as seeding nonlinear search methods.

Relaxed Projection Approach Figure 3-14 depicts the constrained optimization problem in (3.58) and (3.59). It shows the general situation in which the unconstrained optimum solution does not reside within the constrained (i.e., admissible) subspace Ω. In this particular case, the admissible subspace is a convex set [24], defined as

$$\Omega = \{\mathbf{s} : \|\mathbf{s} - \mathbf{s}_{LFM}\| \leq \delta\} \tag{3.60}$$

From Figure 3-14 it is also immediately evident that the admissible waveform closest (in a normed sense) to the unconstrained optimum $\mathbf{s}_{opt}$ lies on the surface of Ω along the direction $\mathbf{i}_o$, which is the unit norm vector that points from $\mathbf{s}_{LFM}$ to $\mathbf{s}_{opt}$, i.e.,

$$\mathbf{i}_o \triangleq \frac{\mathbf{s}_{opt} - \mathbf{s}_{LFM}}{\|\mathbf{s}_{opt} - \mathbf{s}_{LFM}\|} \tag{3.61}$$

Thus, the constrained waveform that is closest in norm to $\mathbf{s}_{opt}$ is given by

$$\hat{\mathbf{s}}_{opt} = \mathbf{s}_{LFM} + \delta \mathbf{i}_o \tag{3.62}$$

Note that if δ is allowed to relax to the point where $\delta = \|\mathbf{s}_{opt} - \mathbf{s}_{LFM}\|$, then $\hat{\mathbf{s}}_{opt} = \mathbf{s}_{opt}$.

EXAMPLE 3.7

Relaxed Projection Example

Here an LFM similarity constraint is imposed on the multipath interference problem considered in Example 3.1. Specifically, in Figure 3-15, we plot the loss in SINR relative to the unconstrained long-pulse optimum solution originally obtained in Example 3.1 as a function

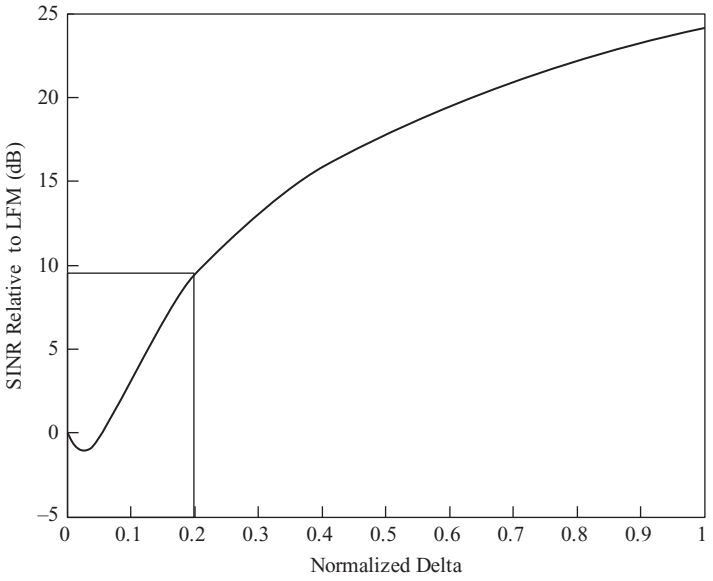

FIGURE 3-15 ■ Illustration of the relaxed projection method for constrained optimization. The plot shows the SINR improvement relative to the unoptimized LFM waveform of example 3.1 versus the normalized relaxation parameter δ. Note that for even a modest relaxation of 20% a nearly 10 dB gain in performance is achieved.

of δ, which is varied between $0 \leq \delta \leq \|\mathbf{s}_{opt} - \mathbf{s}_{LFM}\|$. Note that for this example improvement generally monotonically increases with increasing δ (except for a very small region near the origin) and that sizeable SINR improvements can be achieved for relatively modest values of the relaxation parameter. In other words, a waveform with LFM-like properties can be constructed that still achieves significant SINR performance gains relative to an unoptimized LFM.

Figure 3-16 shows the spectra of the unoptimized LFM of example 3.1 along with the unconstrained optimum and the relaxed projection pulse with a 20% relaxation parameter. Note how the relaxed pulse is significantly closer to the original LFM spectrum yet still achieves nearly a 10 dB improvement in SINR relative to the LFM waveform.

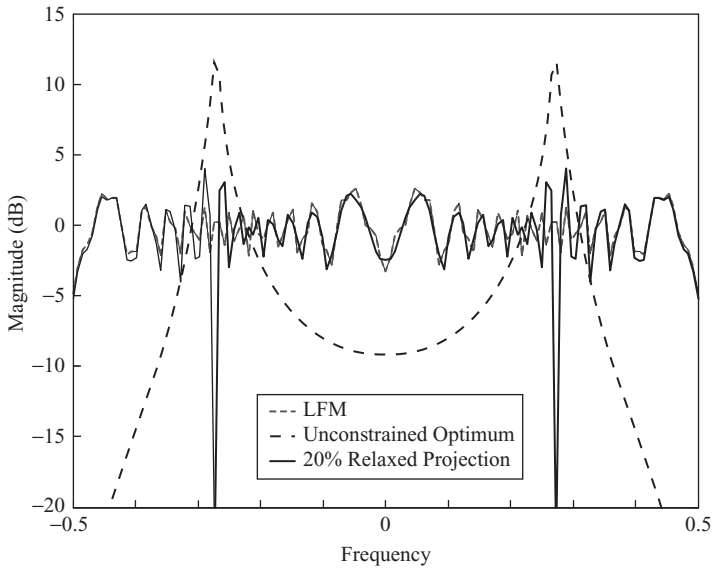

FIGURE 3-16 ■ Comparison of the pulse spectra for the original LFM, unconstrained optimum, and 20% relaxed projection. Note how the relaxed pulse retains LFM-like spectral characteristics (and thus enhanced resolution for example) yet still achieves a 10 dB SINR improvement.

Constant Modulus and the Method of Stationary Phase As has become apparent from the previous examples, spectral shaping plays a key role in achieving matching gains. The stationary phase method has been applied to the problem of creating a nonlinear frequency modulated (NLFM) pulse (and thus constant modulus in the sense that the modulus of the baseband complex envelope is constant, i.e., $|s(t)| = \text{constant}$) with a prescribed magnitude spectrum [5, 12].

Specifically, under fairly general conditions [5, 12] it is possible to relate instantaneous frequency ω of a NLFM waveform to time t [5, 12]:

$$\frac{1}{2\pi}\int_{-\infty}^{\omega} |S(\omega)|^2 d\omega = k\int_{0}^{t} dt = kt \qquad t \in [0, T] \tag{3.63}$$

where $|S(\omega)|$ is the magnitude spectrum of the optimum pulse. Here we have assumed a constant modulus for the NLFM waveform resulting in a integral that is simply proportional to time (see [5, 12] for the more general nonconstant modulus case) as well as a finite and causal pulse.

Solving for ω as a function of t in (3.63) yields the frequency modulation that will result in a transmit pulse with a magnitude spectrum equal to $|S(\omega)|$, to within numerical and other theoretical limitations [5, 12].

EXAMPLE 3.8

NLFM to Achieve Constant Modulus

Here we use the method of stationary phase to design a constant modulus NLFM pulse that matches the magnitude spectrum of the optimum pulse derived for the multipath interference problem considered in Example 3.1.

Figure 3-17 shows the solution to (3.63) (i.e., ω versus t) along with the optimum pulse spectrum from Example 3.1 (long-pulse case). Note that as one would intuit, the frequency modulation dwells at frequencies where peaks in the optimum pulse spectrum occur and conversely note the regions in which the modulation speeds up to avoid frequencies where the optimum pulse spectrum has nulls or lower energy content.

The constant modulus NLFM waveform so constructed was able to achieve an output SINR that was within 6.0 dB of optimum compared with a 24 dB loss using an LFM waveform of same energy and duration.

It is natural to ask if a NLFM waveform with the same spectral magnitude as the optimum pulse (but not necessarily the same phase) will enjoy some (if not all) of the matching gains. For the steady-state case (infinite time duration) this is indeed true, since from Parseval's [5] theorem the output energy is related to only the spectral magnitudes (i.e., without their phases) of the input pulse and channel transfer function, that is,

$$\frac{1}{2\pi}\int_{-\infty}^{\infty} |Y(\omega)|^2 d\omega = \frac{1}{2\pi}\int_{-\infty}^{\infty} |H(\omega)|^2 |S(\omega)|^2 d\omega \tag{3.64}$$

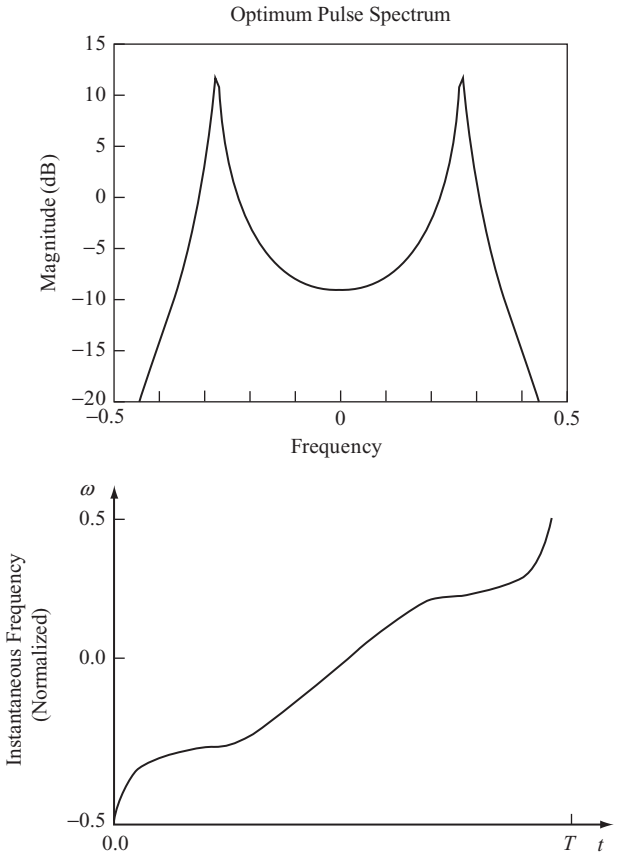

FIGURE 3-17 ■ Illustration of the use of the method of stationary phase to create a constant modulus NLFM pulse whose spectral magnitude matches that of the optimum pulse. The NLFM pulse was able to achieve an output SINR that was within 6.0 dB of the optimum compared with a 24 dB loss using an LFM waveform of same energy and duration.

where $Y(\omega)$, $H(\omega)$, and $S(\omega)$ denote the Fourier transforms of the channel output, channel impulse response, and input pulse, respectively. Note that the output energy in (3.64) depends on the spectral magnitude of the input pulse (steady-state)—not the phase. Thus, in theory an NLFM waveform that exactly matches the optimum pulse magnitude spectrum will achieve the same matching gains in the steady-state limit (infinite pulse duration) for all square integrable (finite norm) functions.

3.6 ADAPTIVE MIMO RADAR

Section 3.2 derived the optimal multidimensional transmit/receive (i.e., MIMO) design equations that assumed exact knowledge (deterministic or statistical) of the channel (target and interference). However, as those familiar with real-world radar are well aware, channel characterization in large part must be performed on the fly, or adaptively. This is simply a result of the dynamic nature of real-world targets and especially interference.

While a plethora of techniques have been developed for radar receiver adaptivity, estimating requisite channel characteristics for adapting the transmit function—especially for transmit-dependent interference such as clutter—is a relatively new endeavor. In this chapter, we explore several approaches for addressing the adaptive MIMO optimization problem.

In Section 3.6.1, we introduce techniques for the case when the channel characteristics are independent of the transmit input—an example of which is additive colored noise jamming. Perhaps not surprisingly, given the transmit independence, the channel estimation techniques are essentially those often invoked in receive-only adaptivity (e.g., STAP [3]).

Section 3.6.2 introduces adaptive MIMO techniques for dynamic transmit array calibration, including the special case of cohere on target. This latter method enables the cohering of RF transmissions of distributed radars for a specific high-value target (HVT) of interest. The methods using the orthogonality approach to waveform design first introduced by Bliss and Forsythe [25] can thus be viewed as a means for estimating the MIMO channel. However, once an estimate of the channel is made, the optimum MIMO transmit/receive functions should be employed.

3.6.1 Transmit-Independent Channel Estimation

As mentioned previously, a multitude of techniques has been developed for the so-called transmit-independent case. A classic example is additive noise jamming [20]. For the case where no a priori knowledge is available, the baseline method of sample covariance estimation—and its many variants such as diagonal loading and principal components [26, 27]—is often used. In addition to its statistical optimality properties (it is the maximum likelihood solution for the i.i.d. additive Gaussian noise case [7]), efficient parallel processing implementations have been developed facilitating its real-time operation [28].

Figure 3-18 depicts a common procedure for estimating additive, transmit-independent interference statistics. Specifically, the interference covariance matrix, $R \in C^{N\times N}$, is approximated by $\hat{R} \in C^{N\times N}$, where

$$\hat{R} = \frac{1}{L}\sum_{q\in\Omega} \mathbf{x}_q \mathbf{x}'_q \tag{3.65}$$

where $\mathbf{x}_q \in C^N$ denotes the N-dimensional receive array snapshot (e.g., spatial, spatiotemporal) corresponding to the q-th independent temporal sample (e.g., a range or Doppler bin), and L denotes the number of i.i.d. samples selected from a suitable set of training samples Ω to form the summation. As depicted in Figure 3-18, this training region is often chosen to be close in range to the range cell of interest (though there are many variants of this). If, moreover, the selected samples are Gaussian and i.i.d., then (3.65) can be shown to provide the maximum likelihood estimate of R [7]. We illustrate this approach in the following example.

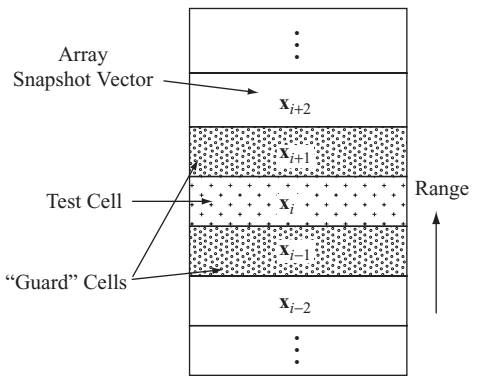

FIGURE 3-18 ■ Illustration of a common method for estimating the interference statistics for the additive transmit-independent case.

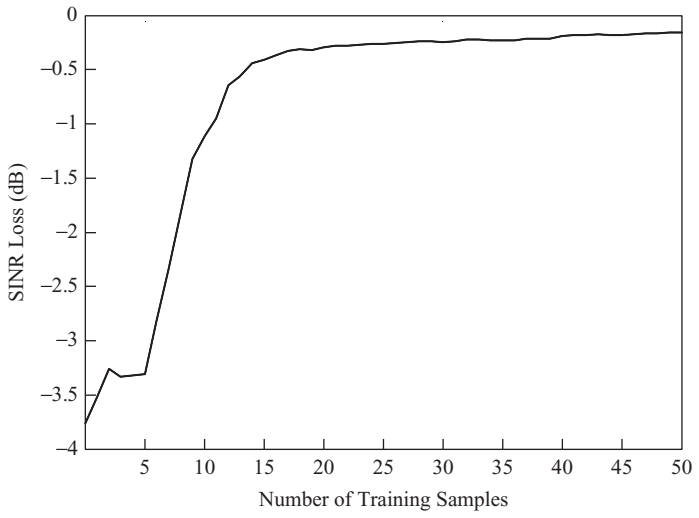

FIGURE 3-19 ■ Effect of sample support on output SINR loss for the multipath interference scenario of example 3.1.

EXAMPLE 3.9

Adaptive Multipath Interference Mitigation

This is a repeat of example 3.1 with the notable exception of unknown interference statistics that must be estimated on the fly. As a consequence, an estimate of the covariance matrix is used in (3.5) for the whitening filter rather than the actual covariance, as was the case in Section 3.2.

Plotted in Figure 3-19 is the overall output SINR loss relative to the optimum for the short-pulse case of example 3.1 as a function of the number of independent samples used in (3.65). The results shown were based on 50 Monte Carlo trials (root mean square average) with a jammer-to-noise ratio of 50 dB and a small amount of diagonal loading to allow for inversion when the number of samples is less than 11 (positive semidefinite case).

It is interesting to note the rapid convergence and contrast this with SINR loss performance for adaptive beamforming, which is generally significantly slower because we are estimating the single dominant eigenvalue–eigenvector pair. For an authoritative examination of principal components estimation and convergence properties, see [29].

3.6.2 Dynamic MIMO Calibration

Perhaps the earliest MIMO radar techniques have their origins in transmit antenna array calibration [30, 31]. While techniques for estimating the receive array manifold using cooperative or noncooperative sources have existed for quite some time [30], methods for dynamically calibrating the transmit array manifold (e.g., AESAs) in situ are relatively recent developments [31].

Figure 3-20 provides an example of using MIMO techniques to dynamically calibrate an AESA radar. Orthogonal waveforms are simultaneously transmitted from each transmit/receive site of an AESA (typically a single subarray AESA). A cooperative receiver then decodes each individual signal, calculates the relative phases (or time delays), and transmits this information back to the radar. By repeating this process for different orientations, a detailed look-up table for the transmit steering vectors can be constructed

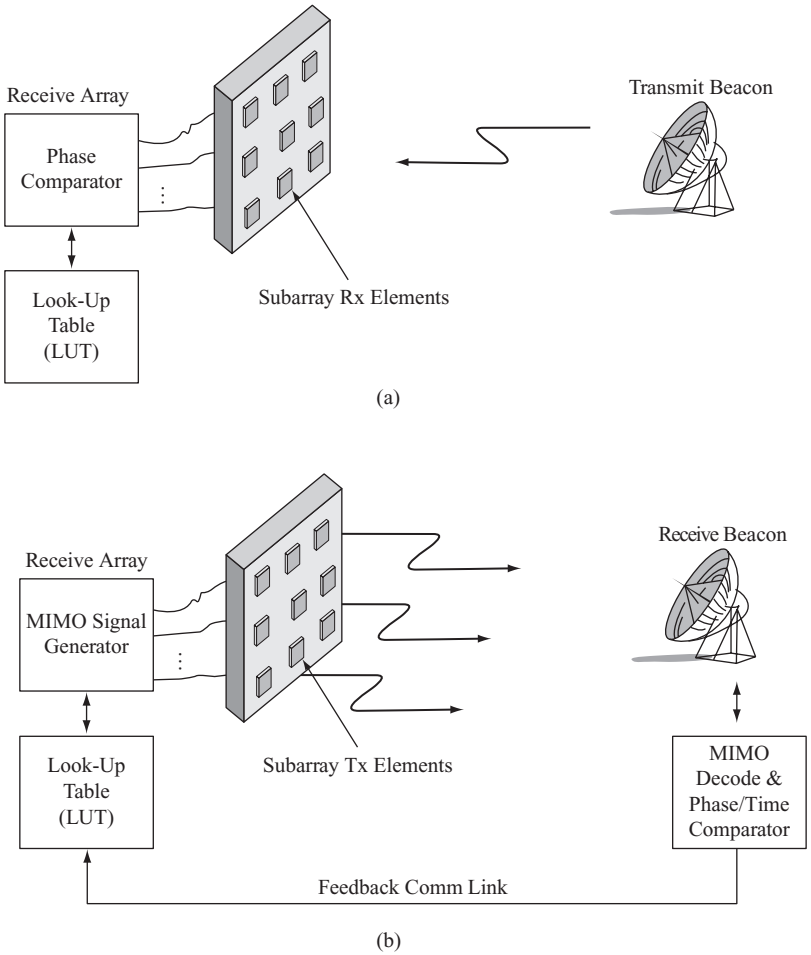

FIGURE 3-20 ■ Illustration of a MIMO-based in situ calibration technique for an AESA radar [30, 31]. (a) Conventional receive array calibration using a known in-band illuminator. (b) The MIMO approach for calibrating the transmit array. (From Steinberg and Yadin [30] and Guerci and Jaska [31]. With permission.)

onboard the radar platform. This in situ approach is basically a necessity for very large AESAs in space since rigidity, which requires mass/weight, is not sufficient to maintain prelaunch calibration [31].

EXAMPLE 3.10

MIMO Cohere-on-Target

An interesting special case of the previously mentioned dynamic in situ calibration procedure is when transmit calibration is performed for a distributed radar focused on a single HVT, as described by Coutts et al. [32].

Consider Figure 3-21, which depicts an airborne HVT that can be detected simultaneously by two geographically disparate radars. Given the HVT nature of the target, it is desired to have the two radars work coherently to maximize the overall SNR at each radar. To achieve on-target coherency, the two waveforms from each radar need to interfere constructively. To accomplish this, however, requires precise knowledge of the transmit pathways to a fraction of a wavelength [32]—essentially a dynamic calibration.

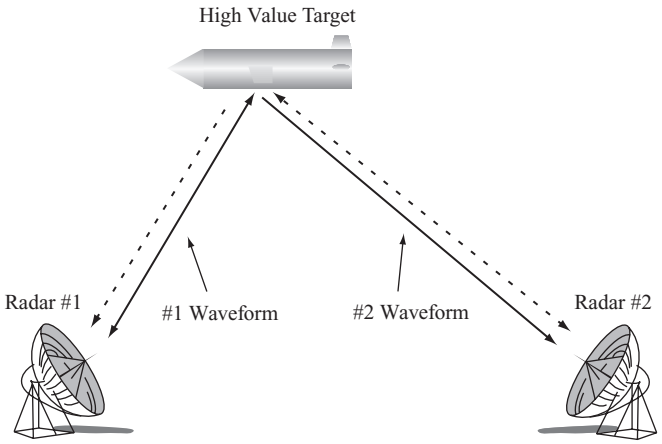

FIGURE 3-21 ■ Illustration of the MIMO cohere-on-target approach for maximizing distributed radar performance. (From Coutts et al. [32]. With permission.)

Drawing on MIMO-based calibration concepts, the requisite relative time delays between the two radars (as seen by the target) can be estimated by simultaneously transmitting orthogonal waveforms, which are then detected and processed in each radar as follows:

- At each radar, the known one-way time delay to the target is subtracted from the total transit time for the sister radar (precise time synchronization is assumed). The remaining time delay is thus due to the first leg of the bistatic path (see Figure 3-21).
- By precompensating a joint waveform in each radar, the two waveforms can be made to cohere on the target—resulting in a 3 dB SNR boost (ideally). If the previous procedure is repeated for N radars, as much as a $10 \log N$ dB gain in SNR is theoretically achievable.

While relatively straightforward to describe, the aforementioned procedure is replete with many real-world difficulties including target motion compensation to a fraction of a wavelength and precise phase and timing stability.

As mentioned previously, the orthogonal waveform MIMO radar approach can provide a means for adaptively estimating the composite target-interference channel since the individual input-output responses can, under certain circumstances, be resolved simultaneously. However, once an estimate of the composite channel is achieved, the optimal MIMO transmit/receive configuration derived in this chapter should be employed to maximize SINR.

3.7 SUMMARY

In this chapter, the fundamental theory for joint optimization of the transmit and receive functions was developed from first principles and applied to the maximization of SINR, SCR, and correct classification for the target ID problem. Constrained optimization was introduced to address additional requirements that often arise in practice, such as the use of constant modulus waveforms to maximize transmitter efficiency. Lastly, basic adaptive methods were introduced to address the real-world issue of estimating the requisite channel information required when it is not available a priori.

3.8 FURTHER READING

Further in-depth details and examples on optimum and adaptive MIMO waveform design, including knowledge-aided methods, can be found in [19]. Further details on the orthogonal MIMO approach can be found in [25].

3.9 REFERENCES

[1] M. A. Richards, *et al.*, *Principles of Modern Radar, Vol I: Basic Principles*. Raleigh, NC: SciTech, 2010.

[2] J. L. Lawson and G. E. Uhlenbeck, *Threshold Signals, volume 24 of MIT Radiation Laboratory Series*. New York: McGraw-Hill, 1950.

[3] J. R. Guerci, *Space-time adaptive processing for radar*. Norwood, MA: Artech House, 2003.

[4] D. K. Barton, *Modern radar system analysis*. Norwood, MA: Artech House, 1988.

[5] A. Papoulis, *Signal analysis*: McGraw-Hill New York, 1984.

[6] A. Papoulis, *Circuits and Systems: A Modern Approach*. New York: Holt, Rinehart and Winston, 1980.

[7] H. L. V. Trees, *Detection, Estimation and Modulation Theory. Part I*. New York: Wiley, 1968.

[8] R. A. Horn and C. R. Johnson, *Matrix analysis*. Cambridge [England] ; New York: Cambridge University Press, 1990.

[9] A. Papoulis and S. U. Pillai, *Probability, random variables, and stochastic processes*: McGraw-Hill New York, 1991.

[10] D. A. Pierre, *Optimization Theory With Applications*: Courier Dover Publications, 1986.

[11] J. R. Guerci and S. U. Pillai, "Theory and application of optimum transmit-receive radar," in *Radar Conference, 2000. The Record of the IEEE 2000 International*, 2000, pp. 705–710.

[12] C. E. Cook and M. Bernfeld, *Radar signals*: Academic Press New York, 1967.

[13] M. A. Richards, *Fundamentals of radar signal processing*: McGraw-Hill, 2005.

[14] M. J. Lindenfeld, "Sparse frequency transmit-and-receive waveform design," *Aerospace and Electronic Systems, IEEE Transactions on,* vol. 40, pp. 851–861, 2004.

[15] S. U. Pillai, *et al.*, "Optimal transmit-receiver design in the presence of signal-dependent interference and channel noise," *Information Theory, IEEE Transactions on,* vol. 46, pp. 577–584, 2000.

[16] D. J. Rabideau, "Closed Loop Multistage Adaptive Beamforming," *Conference Record of the Thirty-Third Asilomar Conference on Signals, Systems and Computers,* pp. 98–102, 1999.

[17] H. L. Van Trees and E. Detection, "Modulation Theory, Part II," ed: New York: John Wiley and Sons, 1971.

[18] H. L. V. Trees, *Detection, Estimation, and Modulation Theory: Radar-Sonar Signal Processing and Gaussian Signals in Noise*: Krieger Publishing Co., Inc., 1992.

[19] J. R. Guerci, *Cognitive Radar: The Knowledge-Aided Fully Adaptive Approach*. Norwood, MA: Artech House, 2010.

[20] R. A. Monzingo and T. W. Miller, *Introduction to Adaptive Arrays*: SciTech Publishing, 2003.

[21] R. Manasse, "The Use of Pulse Coding to Discriminate Against Clutter," *Defense Technical Information Center (DTIC),* vol. AD0260230, June 7, 1961.

[22] W. Y. Hsiang, "On the sphere packing problem and the proof of Kepler's conjecture," *Internat. J. Math,* vol. 4, pp. 739–831, 1993.

[23] W. Gander, *et al.*, "A constrained eigenvalue problem," *Linear Algebra Appl,* vol. 114, pp. 815–839, 1989.

[24] D. C. Youla and H. Webb, "Image Restoration by the Method of Convex Projections: Part 1? Theory," *Medical Imaging, IEEE Transactions on,* vol. 1, pp. 81–94, 1982.

[25] D. W. Bliss and K. W. Forsythe, "Multiple-input multiple-output (MIMO) radar and imaging: degrees of freedom and resolution," presented at the Signals, Systems and Computers, 2003. Conference Record of the Thirty-Seventh Asilomar Conference on, 2003.

[26] B. D. Carlson, "Covariance matrix estimation errors and diagonal loading in adaptive arrays," *Aerospace and Electronic Systems, IEEE Transactions on,* vol. 24, pp. 397–401, 1988.

[27] A. M. Haimovich and M. Berin, "Eigenanalysis-based space-time adaptive radar: performance analysis," *Aerospace and Electronic Systems, IEEE Transactions on,* vol. 33, pp. 1170–1179, 1997.

[28] A. Farina and L. Timmoneri, "Real-time STAP techniques," *Electronics & Communication Engineering Journal,* vol. 11, pp. 13–22, 1999.

[29] S. T. Smith, "Covariance, subspace, and intrinsic Cramer-Rao bounds," *Signal Processing, IEEE Transactions on,* vol. 53, pp. 1610–1630, 2005.

[30] B. D. Steinberg and E. Yadin, "Self-Cohering an Airborne e Radio Camera," *Aerospace and Electronic Systems, IEEE Transactions on,* vol. AES-19, pp. 483–490, 1983.

[31] J. Guerci and E. Jaska, "ISAT - innovative space-based-radar antenna technology," in *Phased Array Systems and Technology, 2003. IEEE International Symposium on*, 2003, pp. 45–51.

[32] S. Coutts, *et al.*, "Distributed Coherent Aperture Measurements for Next Generation BMD Radar," in *Sensor Array and Multichannel Processing, 2006. Fourth IEEE Workshop on*, 2006, pp. 390–393.

[33] P. G. Grieve and J. R. Guerci, "Optimum matched illumination-reception radar," ed: US Patent 5,175,552, 1992.

[34] J. R. Guerci and P. G. Grieve, "Optimum matched illumination waveform design process," ed: US Patent 5,121,125, 1992.

[35] A. Farina and F. A. Studer, "Detection with High Resolution Radar: Great Promise, Big Challenge," *Microwave Journal,* May 1991 1991.

[36] J. R. Guerci, *et al.*, "Constrained optimum matched illumination-reception radar," ed: US Patent 5,146,229, 1992.

3.10 | PROBLEMS

1. A noncasual impulse response can have nonzero values for negative time indices, that is, $h(-k) \neq 0$ for some positive k value. This can arise when the impulse response is not associated with time, such as the case when k is a spatial index or when time samples are processed in batch (buffered) fashion. Rederive the H matrix of equation (3.2) when the impulse response has values from $-M$ to M.

2. Verify that the whitening filter of equation (3.5) (i.e., $H_w = R^{-\frac{1}{2}}$) indeed results in a unity variance diagonal output noise covariance, that is, $\text{cov}(H_w\mathbf{n}) = I$, where $\text{cov}(\cdot)$ denotes the covariance operator. (Hint: H_w is not a random variable and thus is unaffected by the expectation operator.)

3. Assume a target has a transfer matrix given by

$$H_T = \begin{bmatrix} 1 & 1/\sqrt{2} \\ 1/\sqrt{2} & 1 \end{bmatrix}$$

a. What is the optimum input (eigenfunction) that maximizes SNR for the white noise case?

b. If we interpret H_w as a target response polarization matrix in a H–V (horizontal and vertical) basis, what is the optimum polarization direction, assuming H-polarization corresponds to 0 degrees and V corresponds to 90 degrees?

4. The original formulation of equation (3.12) was in the analog domain [33, 34].

a. Assuming the composite channel transfer function (impulse response) is given by the real valued LTI response $h(t)$, show that the optimum transmit function $s(t)$ that maximizes output SNR satisfies

$$\int_0^T s(\tau_2) K(\tau_2, \tau_1) d\tau_2 = \lambda s(\tau_1)$$

where

$$K(\tau_1, \tau_2) \triangleq \int_0^T h(t-\tau_1) h(t-\tau_2) dt$$

and where it is assumed that the pulse duration and receiver integration times are equal to T.

b. Repeat assuming that the impulse response is complex valued.

5. Using MATLAB or some other suitable numerical processing software, compute the H matrices for the short- and long-pulse cases of example 3.1 and verify the results for the optimum transmit waveforms (short and long).

6. Repeat example 3.3 assuming that the target now spans two range bins, that is, $\delta[n] + \delta[n-1]$. Does the result make sense in terms of minimizing interference from clutter?

7. For the two-target optimum ID problem, show that:

a. Maximizing the norm of the separation metric $\mathbf{d} \triangleq \mathbf{y}_1 - \mathbf{y}_2$ in equation (3.42) is statistically optimum for the additive white noise case assuming a unimodal PDF and monotonic distribution function.

b. Extend this to the additive colored noise case (same PDF and distribution assumptions) and show that the separation metric to maximize is now the difference between the whitened target echo responses.

8. The energy in the whitened target echo for the infinite duration case is given by

$$\frac{1}{2\pi} \int_{-\infty}^{\infty} |Y(\omega)|^2 d\omega = \frac{1}{2\pi} \int_{-\infty}^{\infty} |H(\omega)|^2 |S(\omega)|^2 \, d\omega$$

where $Y(\omega)$, $H(\omega)$, $S(\omega)$are the Fourier transforms of the whitened target echo, composite channel transfer function, and input (transmit) waveform, respectively. Show that the input $S(\omega)$ that maximizes the output energy satisfies $|S(\omega)| \propto |H(\omega)|$ [35].

9. A constrained optimum MIMO approach can be developed based on recognizing that the N-dimensional eigenspectrum of the generally positive definite composite channel kernel $H'H$ (or $E\{H'H\}$ for the stochastic case) forms a continuum for which some number k of eigenfunctions (and corresponding eigenvalues) retain matching properties.

a. Assume that k orthonormal eigenfunctions of $H'H$, denoted by $\mathbf{u}_1, \ldots \mathbf{u}_k$, with associated eigenvalues $\lambda_1 \geq \lambda_2 \geq \ldots \geq \lambda_k > 0$, are available and have better matching properties than, say, a nominal nonadaptive quiescent waveform $\mathbf{s}_q$. Derive an expression for the waveform $\mathbf{s}_p$ that resides in the matched subspace spanned by the k best eigenvectors. The resulting waveform can be viewed as a type of constrained optimization in which the properties of the nominal waveform (e.g., good range sidelobes) are traded for better SNR (see, e.g., [36]).

b. Show that in the limit as $k \rightarrow N$, the matched subspace waveform $\mathbf{s}_p \rightarrow \mathbf{s}_q$. (Hint: The eigenfunctions of a positive definite (Hermitian) matrix form a complete basis.)